THE JOURNAL OF BIOLOGICAL CHEMISTRY
Vol. 279, No. 44, Issue of October 29, pp. 46172–46181, 2004

Printed in U.S.A.

A Three-dimensional Model of the Neprilysin 2 Active Site Based on the X-ray Structure of Neprilysin

IDENTIFICATION OF RESIDUES INVOLVED IN SUBSTRATE HYDROLYSIS AND INHIBITOR BINDING OF NEPRILYSIN 2*

Received for publication, June 30, 2004, and in revised form, August 2, 2004
Published, JBC Papers in Press, August 4, 2004, DOI 10.1074/jbc.M407333200

Stéphanie Voisin‡, Didier Rognan§, Claude Gros‡, and Tanja Ouimet‡¶

From the ‡Unité de Neurobiologie et Pharmacologie Moléculaire (INSERM U573), Centre Paul Broca, 2 ter rue d'Alésia, 75014 Paris, France and the §Laboratoire de Pharmacochimie de la Communication Cellulaire (UMR CNRS 7081), Université Louis Pasteur, F-67401 Illkirch, France

Neprilysin 2 (NEP2), a recently identified member of the M13 subfamily of metalloproteases, shares the highest degree of homology with the prototypical member of the family neprilysin. Whereas the study of the *in vitro* enzymatic activity of NEP2 shows that it resembles that of NEP as it cleaves the same substrates often at the same amide bonds and binds the same inhibitory compounds albeit with different potencies, its physiological role remains elusive because of the lack of selective inhibitors. To aid in the design of these novel compounds and better understand the different inhibitory patterns of NEP and NEP2, the x-ray structure of NEP was used as a template to build a model of the NEP2 active site. The results of our modeling suggest that the overall structure of NEP2 closely resembles that of NEP. The model of the active site reveals a 97% sequence identity with that of NEP with differences located within the S'_2 subsite of NEP2 where Ser^{133} and Leu^{739} replace two glycine residues in NEP. To validate the proposed model, site-directed mutagenesis was performed on a series of residues of NEP2, mutants expressed in AtT20 cells, and their ability to bind various substrates and inhibitory compounds was tested. The results confirm the involvement of the conserved Arg^{131} and Asn^{567} in substrate binding and catalytic activity of NEP2 and further show that the modifications in its S'_2 pocket, particularly the presence therein of Leu^{739}, account for a number of differences in inhibitor binding between NEP and NEP2.

Neprilysin 2 (SEP and NL-1) is a recently identified type II membrane-bound zinc-dependent metalloprotease (1–3). It is part of the M13 family of metalloproteases, which also comprises neprilysin (NEP,[1] EC 3.4.24.11) (4–6), the endothelin-converting enzymes, ECE-1 (EC 3.4.24.71) (7) and ECE-2 (8), the Kell blood group antigen (9), the phosphate-regulating neutral endopeptidase on the X chromosome (10) and X-converting enzyme (11). Not only do all of the members of this family of metalloproteases share considerable sequence identities, suggesting a common ancestor as well as a common fold, NEP2, by far the closest homologue of NEP displays over 50% of overall protein sequence identity with NEP, a degree of homology that also suggests a common function (12).

The best characterized member of the family, NEP (13, 14), was first identified as a kidney brush-border neutral endopeptidase slowly hydrolyzing [^{125}I]iodoinsulin B chain (15) and rediscovered as an "enkephalinase" of cerebral membranes hydrolyzing the Gly^3-Phe^4 bond of enkephalins (16). Thereafter, it was shown to hydrolyze a number of biologically active peptides into inactive fragments *in vitro*, such as tachykinins (17), bradykinin (18), and atrial natriuretic peptides (19, 20). The physiological implication of NEP in the inactivation of these messenger peptides was confirmed *in vivo* by the design and use of selective and potent inhibitors, *e.g.* thiorphan (21–24). These functions of NEP and the design of specific inhibitors thereof are of considerable interest, because the inhibitors of NEP have recently been introduced in human gastroenterologic (25) and cardiovascular (26) therapeutic fields.

Whereas NEP is widely distributed in peripheral tissues, NEP2 displays a highly restricted localization expressed exclusively in the central nervous system and testis (1, 27). NEP2 also possesses the particularity of being coded for by a single gene with two major splice variants, one leading to a secreted protein by the insertion of a subtilisin-type cleavage site immediately after the transmembrane domain. This isoform (NEP2(s)) is expressed in round spermatids of the testis (1, 3). The second isoform, mainly expressed in CNS, does not include the subtilisin-type cleavage site and thus leads to a membrane-bound protein (1, 28). Expression of these isoforms in the endocrine corticotrope cell line AtT20 shows that both secreted and membrane-bound isoforms have identical catalytic activities and that they resemble the catalytic activity of NEP insofar, as they have been shown to cleave many of the same substrates, such as tachykinins and enkephalins, at the same amide bonds and with comparable kinetic parameters (28). All of the transition state inhibitors of NEP also inhibit NEP2 activity. Thus, whereas the generic compound phosphoramidon binds both proteases with comparably high affinity (nanomolar range), thiorphan, a specific inhibitor of NEP also inhibits NEP2 at nanomolar concentrations but with an affinity 30 times higher for NEP than for NEP2 (28).

The detailed study of the localization of NEP2 in the nervous system shows that it is widely distributed therein with a generally complementary pattern to that of NEP, although both enzymes are co-expressed in some areas, particularly in the neocortex and red nucleus (1, 27). The most striking complementarity of NEP and NEP2 expression no doubt lies in the basal ganglia where the highest expression of NEP can be

* The costs of publication of this article were defrayed in part by the payment of page charges. This article must therefore be hereby marked "*advertisement*" in accordance with 18 U.S.C. Section 1734 solely to indicate this fact.

¶ To whom correspondence should be addressed. Tel.: 33-1-40-78-92-80; Fax: 33-1-45-80-72-93; E-mail: ouimet@broca.inserm.fr.

[1] The abbreviations used are: NEP, neprilysin; Suc, succinyl; NEP2, neprilysin 2; AMC, amidomethylcoumarin; rNEP2(s), rat-secreted isoform of NEP2; hNEP, human NEP.

observed in caudate putamen and nucleus accumbens, regions that are devoid of NEP2 expression. The high expression of NEP in these regions had already been observed by immunocytochemistry (30) as well as by the quantification of NEP activity (31) and is in accordance with its potential role in the inactivation of endogenous tachykinins (32) and enkephalins of the striatonigral pathway (21). However, this may not exclude a functional role of NEP2 in the inactivation of these neuropeptides, which it efficiently cleaves *in vitro*, because neurons of the striatonigral pathway project upon the substantia nigra pars reticulata, a NEP2-expressing region, devoid of NEP. The identification of NEP2 and the realization that once thought NEP-specific compounds are not as specific as expected bring forward the necessity to reassess the respective functions of NEP and NEP2 in the inactivation of endogenous messenger peptides, particularly in the brain. The design and synthesis of new discriminatory inhibitory compounds will not only constitute useful tools in this endeavor but may be of considerable interest in clinical treatment.

The three-dimensional structure of NEP has recently been elucidated by its co-crystallization with the inhibitory compound phosphoramidon (33). This structure provides a new template to model the structure of metalloproteases of the M13 family clearly superior to the one available thus far, that of the bacterial enzyme thermolysin, which possesses little sequence identity with these mammalian metalloproteases, although it shares considerable similarities in its catalytic activity and inhibitory profile with NEP (34–36). Because of the high sequence identity between NEP and NEP2 and to better characterize the specific pharmacological profile of NEP2 as well as to aid in the design of potent and selective inhibitors of NEP2, we have used the three-dimensional structure of NEP to build and refine a model of the NEP2 active site. The obtained model was validated by site-directed mutagenesis of relevant residues in rNEP2(s), and the expression of these NEP2 mutants in AtT20 cells allowed us to study the impact of such substitutions on the kinetic parameters and affinities of the produced enzymes toward a series of substrates and inhibitory compounds.

EXPERIMENTAL PROCEDURES

Materials—The synthetic fluorogenic substrate Suc-AAF-AMC, dipeptides and related amidated dipeptides, and biological peptides were purchased from Bachem (Voisins le Bretonneux, France). Phosphoramidon was from Sigma (Saint Quentin Fallavier, France), and thiorphan and synthetic compounds I to IV were generous gifts from Denis Danvy and Thierry Monteil (Bioprojet, Paris, France).

Building and Refinement of a Three-dimensional Model of rNEP2—Amino acid sequences of hNEP (Swiss-Prot accession number P08473) and of rNEP2(s) were aligned using the ClustalW multiple alignment program (37). A slow pairwise alignment using BLOSUM matrix series (38) and a gap-opening penalty of 15.0 were chosen for aligning the primary sequences. The three-dimensional model of NEP2 in complex with phosphoramidon was constructed by mutating the side chains of the amino acids in the hNEP-phosphoramidon structure (Protein Data Bank code 1dmt) to the respective side chains in NEP2. Standard geometries for the mutated side chains were given by the BIOPOLYMER module of the Sybyl 6.8 package (TRIPOS Associates, Inc.). Whenever possible, the side chain torsional angles were kept to the values occurring in hNEP. Otherwise, a short scanning of side chain angles was performed to remove steric clashes between the mutated side chain and the other amino acids. Insertions/deletions occurred only in loops but not in secondary structure elements (α-helix, β-sheet). The insertions/deletions in the loops were achieved through a simple knowledge-based loop search procedure using the LOOPSEARCH module of the SYBYL package (TRIPOS Associates, Inc). In this procedure, a set of 1478 high resolution x-ray structures was searched for loops of similar length and similar distance between the Cα atoms of the residues delimiting the loop window. The loop showing the highest homology and the lowest root mean square deviations was then selected for insertion in the model. After the heavy atoms were modeled, all of the hydrogen atoms were added and the protein coordinates were then minimized with AMBER 6.0 (39) using the AMBER95 forcefield (40). The phosphoramidon molecule was parameterized for AMBER 6.0 using a previously described procedure (41). The minimizations were carried out by 2,000 steps of steepest descent followed by conjugate gradient minimization until the root mean square gradient of the potential energy was <0.05 kcal·mol^{-1}·Å^{-2}. A twin cut-off (10.0 and 15.0 Å) was used to calculate non-bonded electrostatic interactions at every minimization step, and the non-bonded pair list was updated every 25 steps. A distance-dependent ($\epsilon = 4r$) dielectric function was used.

Ligand Docking—The three-dimensional coordinates of compound II obtained as previously described (42) were automatically docked into the above-described ligand-free coordinates of NEP2 as well as to those of NEP using 7–8 times speed-up parameters of the GOLD 2.0 docking tool (43). To account for a proper coordination to the zinc ion, a distance constraint was defined between the zinc and the thiol sulfur atom of compound II assuming an intermolecular distance between 1.8 and 2.1 Å and a spring constant of 5 kcal·mol^{-1}·Å^{-2}. To further speed up the calculation, the genetic algorithm docking was stopped when the top three solutions were within a root mean square deviation of 1.5 Å.

Site-directed Mutagenesis of rNEP2(s)—The rNEP2(s)-expressing plasmid, pcDNA-rNEP2(s), has been previously described (28). Double-stranded mutagenesis of rNEP2(s) was carried out using the Transformer site-directed mutagenesis kit (Clontech) following the manufacturer's instructions. All of the constructs were completely sequenced using an automated Licor sequencer to confirm the authenticity of the different mutations as well as the integrity of the NEP2 coding sequence.

Expression of Wild-type and Mutated Forms of rNEP2(s) in AtT20 Cells—AtT20 cells were maintained in Dulbecco's modified Eagle's medium supplemented with 10% (v/v) fetal bovine serum. Transient transfections of wild-type and mutated rNEP2(s) constructs were performed using Superfect (Qiagen, Courtaboeuf, France) according to the supplier's instructions. After 3 h at 37 °C, the transfection medium was replaced by a low protein, serum-free medium, CHO-S-SFM II (Invitrogen). Routinely, the conditioned media were collected 72 h post-transfection and concentrated 10-fold using the centrifugal filter device (Centriprep 30, Amicon). Cells from 140-mm plates were scraped, harvested in ice-cold Hepes buffer (100 mM, pH 7.2, 0.1 mM phenylmethylsulfonyl fluoride) and disrupted with a Polytron (Kinematica, Lucerne, Switzerland). Membranes were obtained by centrifugation (30,000 × *g* for 1 h), resuspended in Hepes buffer, and sonicated (twice for 5 s).

Antibody Production and Immunoblotting—The complete C-terminal region of NEP2 (from residue 83 to 769, see Fig. 1) was amplified using the following oligonucleotides: 5′-GCGAATTCGACATCTGTACTACCCC-3′ and 5′-GCCGCTCGAGTCGATTCATAGGGTGCAT-3′, where nucleotides in *italics* correspond to added EcoRI and XhoI cloning sites, respectively. After digestion with the appropriate restriction enzymes, the amplicon was subcloned into the pET24a vector (a kind gift from Dr. J. C. Barale, Pasteur Institute, Paris, France) and grown in BL21 cells and the corresponding 85-kDa protein was purified and sent to Eurogentech for an immunization protocol.

For immunoblotting experiments, samples were diluted in loading buffer (0.1 M Tris-HCl, pH 6.8, 15% glycerol, 3% SDS, 3% β-mercaptoethanol, 0.02% bromphenol blue), subjected to SDS/PAGE on 7.5% polyacrylamide gels (Bio-Rad), and transferred onto polyvinylidene difluoride membranes (Amersham Biosciences). After 1 h in Tris-buffered saline (0.1 M Tris-HCl, 0.9% NaCl, pH 7.4) containing 0.2% Tween 20 and 5% bovine serum albumin, blots were incubated with the NEP2-specific polyclonal antibody (diluted 1/10,000) for 16 h at 4 °C. Immunoblots were revealed after a 1-h incubation with the appropriate horseradish peroxidase-coupled IgG (diluted 1/3000) using Supersignal (Perbio Science France, Bezons, France).

Enzyme Activity Assays and Inhibitory Potencies—Enzymatic activities of the wild-type and mutated forms of rNEP2(s) were assayed essentially as described in Rose *et al.* (28). For K_m determinations, the incubation mixtures were comprised of 20–50 μg of the concentrated conditioned media and from 7.8 to 1000 μM Suc-AAF-AMC in 100 μl of 100 mM Hepes buffer, pH 7.2, containing 0.15 M NaCl and 0.01% Triton X-100. Incubations were allowed to proceed for 60 min at 37 °C followed by a 60-min incubation with an excess of aminopeptidase M (Pierce) to release fluorescent AMC. The enzyme concentrations were quantified by densitometric analysis of immunoblots using the known amounts of purified NEP2 standards (28).

Inhibitory potencies were determined as follows. After a 15-min preincubation with 20–50 μg of conditioned media and inhibitors or dipeptides in 100 μl of 100 mM Hepes buffer, pH 7.2, containing 0.15 M NaCl, 0.01% Triton X-100, a 20 μM concentration of the model sub-

FIG. 1. **Sequence alignment of the rNEP2(s) and hNEP.** The aligned NEP2 and NEP sequences display 67 and 55% of overall protein sequence similarity and identity, respectively. The amino acids included in the active sites of both enzymes are represented in *boldface* and are *underlined*. Conservative changes are separated by a *single dot*, whereas a *blank space* separates non-conservative substitutions. The zinc-binding HEITH sequence is *shaded*. The percentages of protein similarity and identity within the active site of these proteases are 97 and 86%, respectively. Mutated amino acids are labeled by an *asterisk*.

strate, Suc-AAF-AMC, was added and the reaction was allowed to proceed for 60 min at 37 °C followed by a 60-min incubation with aminopeptidase M. For inhibitory potencies of compounds against NEP, a pure recombinant soluble form of human NEP was used as previously described by Rose *et al.* (28). Inhibitors were tested at concentrations ranging from 1 pM to 10 μM, and peptides from 1 μM to 1 mM. The K_i values were calculated from the IC_{50} values using the Cheng and Prussoff equation.

Statistical Analysis—The Student's *t* tests were performed using the Instat program.

RESULTS

The NEP2 isoforms, NEP2(m) and NEP2(s), are identical in their large C-terminal core, possess identical enzymatic properties, and are inhibited by the same compounds with comparable potencies (28). To ease the study and production of NEP, a secreted form of this enzyme was engineered (secNEP) (44) and was found to have the same enzymatic properties as the natural enzyme. It is this type of construct that was used in the crystallographic study of NEP (33). The model of the active site of NEP2 being based on the alignment of the C-terminal domains of model and template thus applies to both isoforms of NEP2 on one hand as well as to rNEP2 and human NEP2 on the other hand, because both active sites align perfectly (100% sequence identity, data not shown). Coordinates used for NEP2 correspond to rNEP2(s), because this isoform was used in the site-directed mutagenesis studies.

Description of the NEP2 Active Site Model: Comparison to the NEP Active Site Structure—The overall protein sequence similarity between rNEP2(s) and hNEP is of 67% with the highest degree of homology located in the distal C-terminal part of the protein, which contains the active-site consensus sequence HE*XX*H (75% over the last 250 amino acids). Because this high degree of sequence similarity between the two proteins strongly suggests that they have evolved from a common ancestor, we used the recently solved structure of hNEP as a template to build and refine a NEP2 active site model as described under "Experimental Procedures." The three-dimensional structure of NEP2 closely resembles that of NEP, because it is constituted by two domains: the first (domain 1) containing the active site and a second (domain 2) presumably acting as a molecular sieve with both domains separated by interdomain linker fragments (data not shown). Coordinates of phosphoramidon were taken from the respective hNEP complex and merged into the NEP2 model. The active site of both enzymes was then designed as any amino acid included into a 6-Å radius sphere centered on the inhibitor. The NEP2 active site model thus obtained was highly similar to the hNEP structure, both active sites displaying 97 and 86% amino acid sequence similarity and identity, respectively (Fig. 1).

The conserved zinc binding motif, HEITH, from template and model is well superimposed. The zinc ion is coordinated in an approximately tetrahedral geometry (Fig. 2*A*), and its binding involves a single oxygen atom of the tetrahedral N-phosphoryl moiety of the inhibitor and three ligands from the protein: His^{608}; His^{612}; and Glu^{671} for NEP2, respectively (His^{583}, His^{587}, and Glu^{646} for hNEP).

The catalytically important residues involved in inhibitor binding from template and model are perfectly matched. For instance, Arg^{742} of NEP2 (Arg^{717} in hNEP) interacts with the inhibitor by forming a hydrogen bond with the carbonyl oxygen atom of the L-leucyl residue in the P'_1 position, the carbonyl

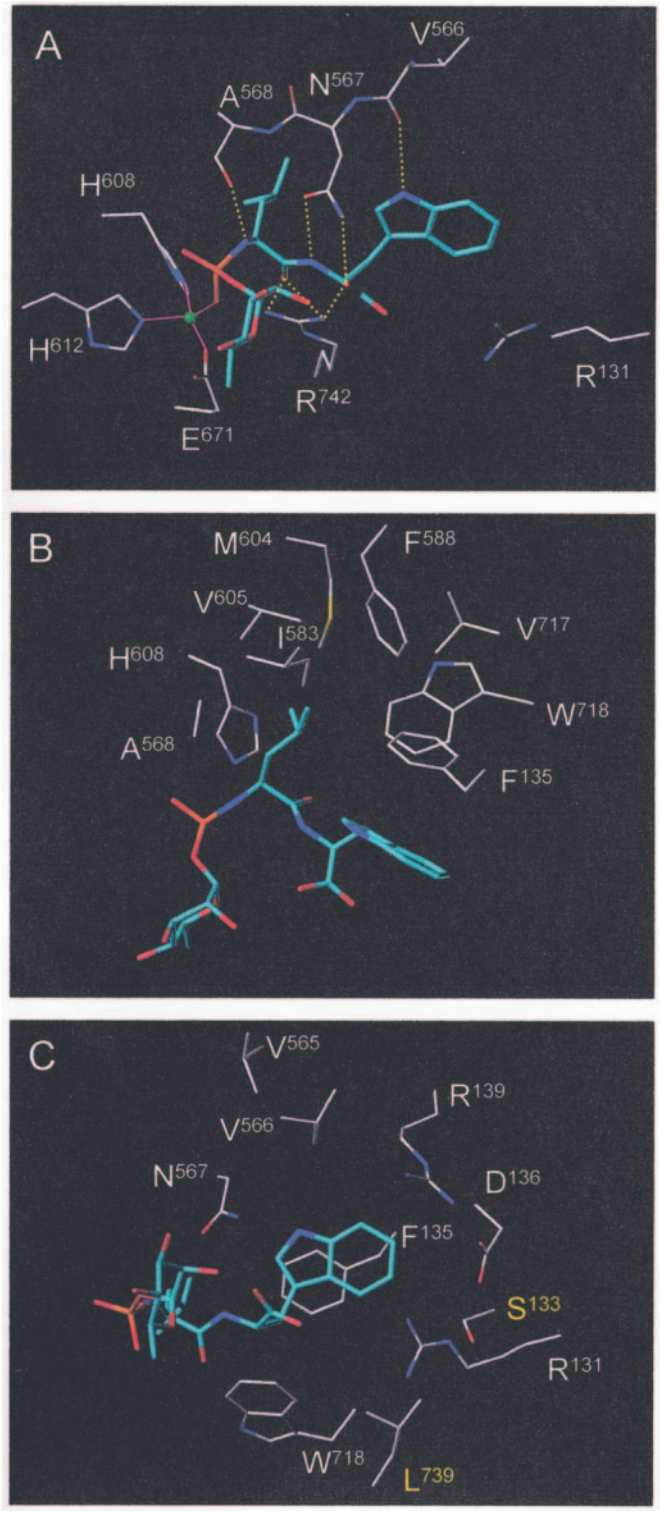

FIG. 2. **Three-dimensional model of the NEP2 active site based on the NEP crystal structure.** A proposed model of the NEP2 active site and of its interactions with the inhibitory compound phosphoramidon is shown. *A*, network of hydrogen bonds and coordination to the Zn^{2+} atom. *B*, close-up of interactions between the P'_1 side chain and the S'_1 subsite. *C*, close-up of interactions between the P'_2 side chain and the S'_2 subsite. Carbon atoms of the enzyme and of the inhibitor are displayed in *white* and *cyan*, respectively. Otherwise, the following color code is used: oxygen atom, *red*; nitrogen atom, *blue*; phosphorus atom, *orange*; and sulfur atom, *yellow*. Intermolecular hydrogen bonds are shown as *yellow dots*. Coordination to the Zn^{2+} atom (*green ball*) is represented by *magenta lines*. Enzyme residues are labeled at their Cα atom. Positions mutated herein are labeled in *yellow*.

oxygen atom of Ala^{568} of NEP2 (Ala^{543} in hNEP) is hydrogen-bonded with the peptide amide group of the P'_1 residue of phosphoramidon, and the side chain of Asn^{567} of NEP2 (Asn^{542} in hNEP) forms two hydrogen bonds with the amide and carboxyl groups of the P'_2 residue of the inhibitor (Fig. 2*A*). Additionally, the side chain of Arg^{131} of NEP2 (Arg^{102} in hNEP) does not allow a direct hydrogen bond but may form a two water-mediated interaction with the terminal carbonyl group of the inhibitor as in hNEP.

NEP and NEP2 cleave peptidic substrates at the N terminus of aromatic or large hydrophobic residues, which constitute the P'_1 amino acid in the P_2-P_1-P'_1-P'_2 commonly accepted Schechter and Berger nomenclature. The specificity of these enzymes is therefore the result of specific interactions of the P'_1 and P'_2 side chains within the S'_1 and S'_2 subsites of the enzyme. The S'_1 subsites of the NEP2 model and hNEP template are quasi-identical. They form a large hydrophobic pocket containing the side chains of Phe^{135}, Ala^{568}, Ile^{583}, Phe^{588}, Met^{604}, Val^{605}, His^{608}, Val^{717}, and Trp^{718} for NEP2 (Phe^{106}, Ala^{543}, Ile^{558}, Phe^{563}, Met^{579}, Val^{580}, His^{583}, Val^{692}, and Trp^{693} for hNEP, respectively) (Fig. 2*B*). There is a single amino acid difference between model and template in this subsite (Tyr^{714} for NEP2 (Phe^{689} in hNEP)), but this amino acid lies in the far end of the pocket and does not directly interact with the inhibitor.

However, more important differences between model and template were observed in the region of the S'_2 subsite. In the hNEP structure, the side chains of Arg^{102}, Asp^{107}, and Arg^{110} form this pocket but in the NEP2 model, even if the respective amino acid side chains of Arg^{131}, Asp^{136}, and Arg^{139} are equally present, the ones of Ser^{133} and Leu^{739} are found at positions filled by two glycine residues, Gly^{104} and Gly^{714}, in hNEP (Fig. 2*C*). On one hand, the side chain of Ser^{133} and, more significantly, that of Leu^{739} should occupy more space than their corresponding Gly^{104} and Gly^{714} residues in hNEP and/or, on the other hand, change the binding of substrates or inhibitors. Another amino acid, Phe^{726} (Tyr^{702} in hNEP), differs between model and template in this subsite, but it is located far at the bottom of the S'_2 pocket.

The phosphoramidon-NEP2 active site complex model allows us to propose a schematic representation of the peptidic substrate interactions with NEP2 (Fig. 2*A*), a model in which overall these interactions are highly similar to those of NEP. However, the results presented here bring forward the fact that the S'_2 subsite of NEP2 may differ from that of NEP due to the presence of the Ser^{133} and particularly Leu^{739} in lieu of the two glycine residues found in the corresponding positions of the NEP sequence, substitutions which may contribute to the pharmacological differences between the two proteases.

Exploration of the S'_2 Subsite of NEP2 by Site-directed Mutagenesis of rNEP2(s)—We have recently shown that NEP2 isoforms expressed in AtT20 cells are synthesized in the endoplasmic reticulum as inactive precursors of 110 kDa, which must exit this compartment in order to become active. The activation of the NEP2 isoforms is concomitant with their acquisition of complex sugars reflected by an increase in their molecular weights. In the case of rNEP2(s), membranes only express the inactive 110-kDa form, whereas the mature and active enzyme is entirely recovered in the medium as a 125-kDa protein. Enzymatic activity of wild-type rNEP2(s) thus is detected exclusively in the conditioned media of transfected AtT20 cells and can be monitored using the fluorogenic model substrate Suc-AAF-AMC (28). Because no significant differences between the S'_1 subsites of NEP and NEP2 were observed, the S'_2 subsite, the region in which differences between the two metalloproteases were brought to light by the here

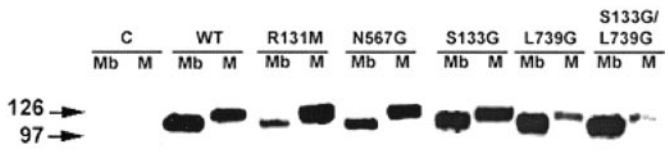

FIG. 3. **Immunoblot analysis of membranes and conditioned culture media from wild-type and mutated rNEP2(s)-transfected AtT20 cells.** 30 μg of total protein from membrane preparations (*Mb*) and conditioned culture media (*M*) from control (*C*), wild-type (*WT*), and mutated rNEP2(s)-transfected AtT20 cells were separated on a 7.5% SDS-polyacrylamide gel under reducing conditions and immunoblotted with a NEP2-specific polyclonal antibody. Membrane fractions contain an immunoreactive band of 110 kDa corresponding to inactive NEP2, whereas the conditioned media display a 125-kDa protein that corresponds to fully glycosylated, secreted, and active NEP2.

exposed modeling, was further explored by site-directed mutagenesis using the secreted isoform, rNEP2(s), as a template. Four amino acids were chosen: two identical to NEP (Arg^{131} and Asn^{567}) and the two differing between NEP and NEP2, *i.e.* Ser^{133} and Leu^{739}.

Constructs coding for wild type, rNEP2(s)-R131M, or rNEP2(s)-N567G were transiently transfected in AtT20 cells, and the presence of the enzyme in the membrane fraction and/or in the conditioned culture media was determined by Western blot analysis. These results show that the wild-type form of rNEP2(s), as previously reported (28), is expressed both in the membrane fraction and in the conditioned medium of transfected AtT20 cells as either a 110-kDa membrane-bound protein or an ~125-kDa band in the conditioned medium (Fig. 3). Mutants of the S'_2 subsite, rNEP2(s)-R131M and rNEP2(s)-N567G, produced the same molecular weight bands when expressed in AtT20 cells, suggesting normal processing of these proteins (Fig. 3). Furthermore, as shown in Table I, the introduction of these mutations in the NEP2 active site produced enzymatically active proteases, however, with altered catalytic properties.

Kinetic values of rNEP2(s)-R131M were not different from wild type using the model substrate Suc-AAF-AMC in which the AMC molecule blocks its C-terminal end. Indeed, neither the K_M ($p = 0.21$) nor the k_{cat} ($p = 0.18$) of this mutant toward the fluorogenic model substrate is significantly different from wild type. Further exploration of the catalytic site of this mutant using inhibitory dipeptides (Table II), however, uncovers the role of Arg^{131} in substrate binding, which in the proposed model (Fig. 2*A*) is hydrogen-bonded to the C-terminal group of the peptidic substrate or inhibitor. Dipeptides are considered inhibitory because they bind the active site of metalloproteases in the S'_1 and S'_2 subsites and thus inhibit their catalytic activity monitored here with the model fluorogenic substrate. Inhibitory potencies of dipeptides or their respective amidated counterparts were determined against wild type and the R131M mutant (Table 2). On one hand, inhibitory potencies of natural dipeptides were significantly decreased against rNEP2(s)-R131M as compared with the wild-type enzyme (6-fold decrease for Val-Phe ($p = 0.044$) and a 4.5-fold one for Leu-Met ($p = 0.023$), reflecting a decrease in the affinity of these dipeptides toward the mutant. On the other hand, although rNEP2(s)-R131M showed no preference for the natural dipeptides over their amidated forms ($p \geq 0.5$), wild-type rNEP2(s) displayed a strong decrease in its binding of amidated Leu-Met or Val-Phe (a 9-fold ($p = 0.0061$) and 6-fold ($p = 0.0036$) decrease, respectively), reaching comparable values as those obtained for rNEP2(s)-R131M, clearly demonstrating that peptide amidation abrogates binding of the P'_2 residue to Arg^{131} but not the binding of the dipeptide itself. The involvement of Arg^{131} in the binding of residues in P'_2 was further confirmed by the study of the affinities reflected by their inhibitory potencies (K_i) against the model fluorogenic substrate of a series of bioactive peptides previously shown to be efficiently cleaved by NEP2 (28). As for amidated dipeptides, the binding of substance P or cholecystokinin-8, both naturally amidated peptides, was unaffected by the mutation (Table III). In the same manner, wild-type rNEP2(s) displayed a significant ($p = 0.0046$) 11-fold preference for [Leu^5]enkephalin over its amidated counterpart, a preference that was lost to the rNEP2(s)-R131M mutant (Table III). The angiotensin I or bradykinin affinities were equally unaffected by the loss of the Arg^{131} residue in NEP2. These results show that Arg^{131} is not involved in the binding of substrates, which are subject to endoproteolysis (reflected by angiotensin I cleavage) as opposed to those cleaved by the dipeptidyl carboxypeptidase activity of NEP2 (*e.g.* [Leu^5]enkephalin and CCK1–6) whose binding is affected by the loss of this charged residue. However, the observed results suggest that Arg^{131} does not play an essential role in this latter activity as P'_2 residues, which cannot form any hydrogen bond with it (because of charge repulsion) (*i.e.* the ultimate arginine residue of bradykinin), bind with high affinity, the active site of NEP2 or of its R131M mutant (Table III). Taken together, these results show that the R131M mutation does not affect the integrity of the rNEP2(s) structure and strongly argue for a role of Arg^{131} in the binding of the free

TABLE I

Comparison of the kinetic constants of wild-type and mutant forms of NEP2 using the model fluorogenic substrate Suc-AAF-AMC

Enzyme-substrate incubations were performed at 37 °C for 60 min followed by a 60-min incubation in the presence of aminopeptidase M to release fluorescent AMC. K_M values are the mean values of at least three independent determinations. NEP values towards this same model substrate have previously been reported (a K_M of 70 μM and k_{cat} of 2,200). In this same paper, we had found a mean K_M value of 50 μM and a k_{cat} of 510 for NEP2 (28), *i.e.* comparable to the results obtained here. The wild-type NEP specificity constant has previously been compared with those of its R102M and N542G mutants (the NEP equivalents of Arg^{131} and Asn^{567} in NEP2) by Dion *et al.* (46), who have reported them to be of 9.33, 5.24, and 0.523, respectively, using [tyrosyl-(3,5-^{3}H)](D-Ala^2)-Leu^5-enkephalin as substrate.

NEP2	K_M	k_{cat}	k_{cat}/K_M
	μM	min^{-1}	$\mu M^{-1} \cdot min^{-1}$
Wild-type	62 ± 9	842 ± 72	13
R131M	45 ± 7	1038 ± 107	23
N567G	1000	314 ± 31	0.3
L739G	40 ± 6	1840 ± 164	46
S133G	185 ± 34	118 ± 18	0.6
L739G+S133G	44 ± 5	1140 ± 117	26

TABLE II

Inhibitory potencies of free versus amidated dipeptides towards wild-type rNEP2(s) and its R131M mutant

Catalytic activity of wild-type or mutated NEP2 towards the fluorogenic model substrate Suc-AAF-AMC was inhibited by increasing concentrations of free or amidated dipeptides to measure their binding affinities. Numbers are mean values of at least three independent determinations. The results obtained with this NEP2 mutant are comparable to previously published results with the equivalent NEP mutant. Indeed, a NEP-R102M mutant has been shown to display decreased affinity towards an X-Phe dipeptide, compared with the wild-type enzyme (5.5-fold) (46) whereas amidation of dipeptides has been shown to have the same effect as those displayed here (49).

Peptides	K_i	
	rNEP2(s)	R131M
	μM	
Val-Phe	21 ± 5	135 ± 39
Val-Phe-NH_2	130 ± 20	100 ± 25
Leu-Met	20 ± 4	90 ± 19
Leu-Met-NH_2	175 ± 25	116 ± 42

TABLE III

Binding affinity of various NEP2 bioactive peptidic substrates towards wild-type and R131M NEP2

A 20 μM concentration of fluorogenic substrate Suc-AAF-AMC was used to evaluate the inhibitory potencies of various biological peptides previously described as NEP2 substrates. K_i values thus obtained are the reflection of their affinities towards the enzyme. The arrows represent the sites of cleavage of NEP2 as previously determined by high pressure liquid chromatography (28). Full arrows correspond to the preferential NEP2 cleavage sites.

Peptides	Séquence	Ki (μM)	
		RNEP2(s)	R131M
Substance P	RPKPQQ ↓ – FFG ↓ – LM-NH_2	11 ± 4.0	8 ± 1.5
Angiotensin I	DRVY ⇣ – IHP ↓ – FHL	8 ± 2	8 ± 2
Bradykinin	RPPGFSP ↓ – FR	3 ± 0.5	2.5 ± 0.7
[Leu^5]-enkephalin	YGG ↓ – FL	2 ± 0.6	65 ± 11
[Leu^5]-enkephalin-NH_2	YGG ↓ – FL-NH_2	20 ± 5	52 ± 20
Cholecystokinin-8 (nonsulphated)	DYMG ↓ – WMDF-NH_2	10 ± 2	21 ± 8
Cholecystokinin(1-6)	DYMG ↓ – WM	50 ± 5	> 300

carboxylate group of substrates, although this binding is dependent on the nature of the P'_2 residue and of its interactions within the S'_2 subsite.

Expression of rNEP2(s)-N567G in AtT20 cells and study of its catalytic activity using the model substrate showed that the K_M of this mutant toward the fluorogenic substrate was significantly increased ($p \leq 0.001$) as compared with the wild type enzyme, whereas its k_{cat} decreased by ~3-fold ($p = 0.0005$), yielding an enzyme with a 43-fold decrease in its specificity constant (Table I). The significant effect of this mutation on the catalytic parameters of NEP2, on one hand, confirms the critical role of the Asn^{567} residue in hydrolysis and in binding of the substrate as had been previously demonstrated for NEP (46) and, on the other hand, lends further credence to our proposed model of the NEP2 active site.

To further test our model, the side chains of the Ser^{133} and Leu^{739} residues of the S'_2 subsite of NEP2 were replaced by glycine residues to explore whether the produced enzyme would acquire a NEP-like pharmacological profile. The expression of rNEP2(s)-S133G, rNEP2(s)-L739G, and that of the double mutant rNEP2(s)-S133/L739G in AtT20 cells followed by immunoblotting experiments revealed that these constructs produced normally secreted NEP2 proteins (Fig. 3). However, although these mutant forms of rNEP2(s) possessed enzymatic activity, the K_M of rNEP2(s)-S133G was significantly increased ($p = 0{,}025$), whereas its k_{cat} was reduced 7-fold ($p = 0.001$), yielding an enzyme with a 22-fold decrease in its specific activity, suggesting an effect of this mutation both in substrate binding as well as on hydrolysis (Table I). On the contrary, the rNEP2(s)-L739G and the double mutant displayed specificity constants toward the model fluorogenic substrate increased by 3.5- and 2-fold, respectively, reaching values comparable to those of NEP previously determined in the same conditions to be ~30 (Table I) (28). Moreover, this increase of the specificity constant was essentially the result of an increase in k_{cat} (although only the increase of the k_{cat} of L739G reaches significance ($p = 0.014$) suggesting that, although the binding of the substrate is not affected by these mutations, the catalytic activity is increased (Table I).

To explore the influence of the Ser^{133} and Leu^{739} residues of the S'_2 subsite of NEP2 on inhibitor binding, K_i values of various synthetic compounds were determined against these mutants and compared with those of wild-type NEP2 and NEP (Table IV). Moreover, to assess the specific role of these residues in the pharmacological differences between NEP2 and NEP, the effects of the S133G and L739G mutations were also compared with those of residues equivalent in NEP2 and NEP, *i.e.* the R131M and N567G mutants (Arg^{131} corresponding to Arg^{102} in NEP and Asn^{567} to Asn^{542}). As previously shown (28), all of the transition-state inhibitors of NEP inhibit NEP2 activity, although both metalloproteases do not display an identical pharmacological profile. Thus, phosphoramidon and compound III are strong equipotent inhibitors of both peptidases (~1 nM for phosphoramidon and 0.5 nM for compound III). However, in the cases of thiorphan compounds I, II, and IV, the K_i values strongly differ between NEP and NEP2 (K_i rNEP2(s)/K_i hNEP = 30 for thiorphan, 14 for compound I, 600 for compound II, and 60 for compound IV).

TABLE IV

Inhibitory potencies of a series of compounds against wild-type and mutant forms of NEP2 compared to NEP

The model fluorogenic substrate Suc-AAF-AMC (20 μM) was used to evaluate the inhibitory potencies of a series of compounds systematically modified in P'_1 and P'_2 based on the structure of thiorphan against the activities of mutants of the rNEP2(s) S'_2 subsite. These values are also compared with NEP. Numbers the are mean values of at least two independent determinations. K_i values of the double S133G/L739G NEP2 mutant in boldface are statistically different from wild type.

Compounds	Ki (nM)						
	NEP	NEP2	R131M	N567G	S133G	L739G	S133G/ L739G
Phosphoramidon 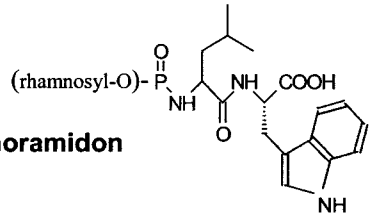	1.5	1.0	6.0	3.0	4.1	1.5	1.1
Thiorphan 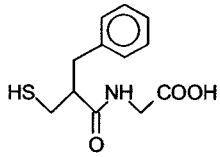	4.0	120	>1000	55.5	700	150	130
Compound I 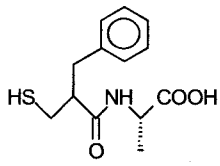	1.0	14.1	6.3	60.0	10.5	5.1	**3.3**
Compound II 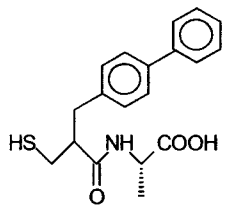	0.1	60	>1000	32.0	210	0.6	**0.2**
Compound III 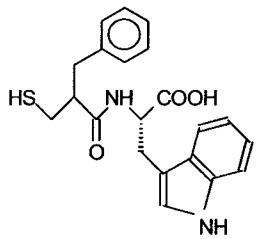	0.4	0.5	1.5	4.2	0.1	0.1	**0.1**
Compound IV 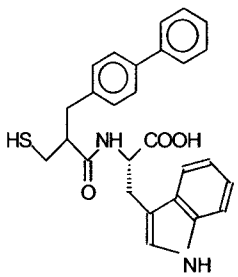	1.3	80	44.2	28.9	6.3	0.8	**0.3**

Whereas the inhibitory potencies of all of the compounds tested against the rNEP2(s)-N567G mutant were modified, no tendency of a change toward NEP values could be detected (Table III). Although the same observation can be made for the R131M mutant, it is interesting to note that the mutation of this residue had a severe impact on the binding of two compounds, thiorphan and compound II (Table III), suggesting that this residue is also involved in inhibitor binding in NEP2.

Phosphoramidon, an equipotent compound against NEP and NEP2, did not display any significant change in its affinity toward the rNEP2(s)-S133G, rNEP2(s)-L739G, and rNEP2(s)-L739G+S133G mutants. However, in the case of compound III, the second equipotent compound tested, a significant decrease in its K_i value toward the double S133G/L739G mutant ($p = 0.0176$) was observed, a value that furthermore became slightly different from that of NEP ($p = 0.43$), toward a better affinity. These results show that identical S'_2 subsites, as defined by co-crystallization on one hand and our modeling on the other, can bind a given compound differently, thus suggesting cooperativity in the various subsite interactions of a given compound as other interactions must come into play in or outside this S'_2 subsite mutant of NEP2 for it to bind compound III with a higher affinity than NEP.

Variations of K_i values of the NEP2(s) mutants toward NEP values are observed among the discriminating compounds, the only exception being thiorphan whose inhibitory potency toward the NEP2 double mutant is identical to that of wild-type NEP2 ($p = 0.82$). Indeed, the K_i values of compounds I and IV toward the rNEP2(s)-S133G mutant are decreased toward values obtained with NEP, although results obtained with this mutant are not as flagrant as those obtained with rNEP2(s)-L739G. The inhibitory potencies of compounds I, II, and IV against the L739G NEP2 mutant are almost identical to those of NEP, confirming in a clear-cut manner the contribution of Leu^{739} in the pharmacological differences between NEP and NEP2. Although the result obtained with the S133G mutant are to be taken cautiously because of its decreased specific activity, it is interesting to note that the K_i values obtained with the double mutant (rNEP2(s)-S133G/L739G), which produces an active enzyme with kinetic values comparable to those of rNEP2(s)-L739G, are always lower than those of NEP2 proteins containing either mutation alone, suggesting some kind of cooperative effect of the Ser^{133} and Leu^{739} residues in inhibitor binding. Indeed, using the discriminating NEP/NEP2 compounds, the obtained K_i values toward the NEP2 double mutant on one hand are significantly different from the ones against wild type NEP2 ($p = 0.035$, 0.001, and 0.016 for compounds I, II, and IV, respectively). On the other hand, these same values are the reflection of the acquired NEP-like properties of the NEP2 double mutant as they reach values either statistically indistinguishable from those of NEP ($p = 0.056$ and 0.14 for compounds I and II, respectively), or, in the case of compound IV, 4-fold better than against NEP ($p = 0.12$), once again bringing to light the importance of other unidentified subsite interactions.

DISCUSSION

Until recently, the only structure available for the modeling of zinc-metalloproteases of the M13 subfamily was that of thermolysin, which, has little sequence homology with these proteases, although it shares many enzymatic properties with NEP and a common active site structure (34–36). Therefore, it constitutes a poor template, seeing it is a distant bacterial enzyme (from *Bacillus stearothermophilus*) that does not contain all of the catalytically important residues of NEP, and is significantly shorter in length than NEP and its homologues (316 amino acids for thermolysin *versus* 743 for hNEP). The recent disclosure of the structure of the ectodomain of NEP obtained by x-ray crystallography (33) provides a new and relevant template to model closely related members of the M13 subfamily and, in particular, the recently characterized NEP2 neuropeptidase (1–3). The obtained active site model of NEP2 (Fig. 2) shows that the structure of these two metalloproteases share many features as expected, on one hand, by their high sequence identity (1) and, on the other hand, by their similar specific activities and inhibitory profiles (28). In this respect, zinc coordination in the NEP2 model is achieved by His^{608}, His^{612}, and Glu^{671} (His^{583}, His^{587}, and Glu^{646} in hNEP) and all of the amino acids defined by Oefner *et al.* (33) as involved in hydrolysis and inhibitor (or substrate) binding in NEP are also conserved in NEP2, similar to Arg^{133}, the $^{566}VNA^{568}$ motif (which can be extended to $^{566}VNA(F/Y)Y^{570}$), Glu^{671}, His^{736} (which is involved in the stabilization of the transition state of NEP (45) and is hydrogen-bonded to Asp^{734}), and to Arg^{742} (Arg^{102}, $^{541}VNA^{543}$, Glu^{646}, His^{711}, Asp^{709}, and Arg^{717} in hNEP, respectively). The definition of the organization of these amino acids into subsites further reveals that, whereas the S'_1 subsite of NEP2 and NEP are basically constituted by the same residues, their S'_2 subsites contain amino acid substitutions that could account for pharmacological differences between these two proteases. Indeed, in this subsite, the NEP and NEP2 metalloproteases differ by two amino acids with Ser^{133} and Leu^{739} replacing two glycine residues in NEP, a difference that warranted further exploration of this subsite by site-directed mutagenesis.

For these experiments, we used the secreted isoform of NEP2 (NEP2(s)), which naturally sheds its C-terminal domain in the extracellular milieu (28) and which corresponds to the genetically engineered form of NEP produced for its x-ray crystallographic study (secNEP) (44, 28). Mutation of the Arg^{131} or Asn^{567} residues of the NEP2 active site to methionine or glycine, respectively, yielded active, normally secreted NEP2 mutants (Fig. 4 and Table I). As proposed in our model, the results displayed in Tables I and II suggest a similar role of these two amino acids in NEP2 and NEP (Fig. 2). Indeed, the mutation of these residues in NEP (46) had previously shown a stronger interaction of Asn^{542} than Arg^{102} with the substrate. The 10-fold decrease in affinity of the rNEP2(s)-N567G mutant toward the model substrate confirms the involvement of this residue in substrate binding with this effect being furthermore comparable to a ~14-fold decrease in affinity observed for a NEP-N542G mutant (45–46). Hydrolysis was also affected by the introduction of the N567G mutation within the NEP2 sequence, underlying the critical role of this residue in catalytic activity. Whereas the Asn^{567} residue is revealed to be essential to the NEP2 catalytic activity, the effects of the R131M mutation were more subtle as they were, for example, not significant on model substrate activity (Table I). However, NEP and NEP2 have been shown to possess a dipeptidyl carboxypeptidase activity (47, 48, 28) and, in NEP, Arg^{102} was demonstrated to bind the free carboxylate of substrates (or inhibitors) and thus direct cleavage toward their C-terminal end (46, 48–50). Of the various Arg^{102} NEP mutants previously produced, an R102M mutant tested against various Phe-*X* dipeptides showed that their inhibitory potencies were generally decreased by this mutation compared with wild-type NEP (46), as observed here for NEP2 (Table II). The affinity of Phe-Gly toward NEP, the binding of which was of the most severely affected by the mutation of Arg^{102}, decreased from the micromolar to millimolar range for wild-type and R102M NEP mutant, respectively, a difference in binding observed with NEP2 and thiorphan, which is constituted by a phenylalanine in P'_1 and a glycine residue in P'_2 (Table IV) (46). The loss of this active site arginine residue in both NEP and NEP2 (Arg^{102} or Arg^{131}, respectively) has an equivalent impact on the binding of P'_2 phenylalanine residues (5.5- *versus* 6-fold decrease in the binding of *X*-Phe to NEP and to NEP2, respectively), and the binding of enkephalins to NEP has also been shown to be compromised by the loss of Arg^{102} in NEP (46, 48) as demonstrated here for [Leu^5]enkephalin as well as for cholecystokinin 1–6 using the rNEP2(s)-R131M mutant. Although amidation of

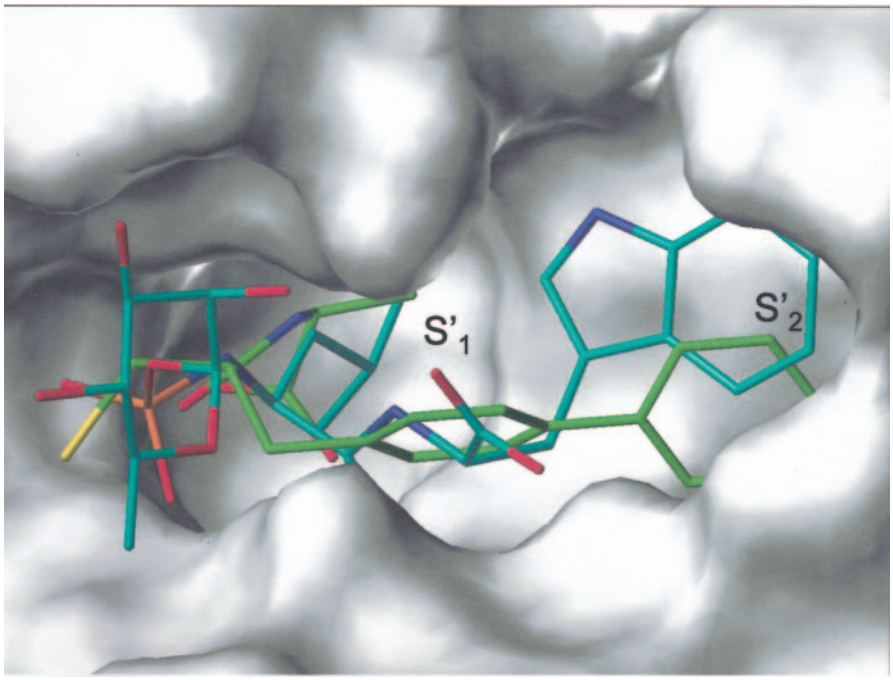

FIG. 4. **Docking of compound II to the hNEP x-ray structure.** The best GOLD solution (fitness score of 55.97) of compound II (*green sticks*) is displayed with respect to the hNEP-bound phosphoramidon crystal coordinates (*cyan sticks*). The location of the S'_1 and S'_2 sites is marked on the enzyme water-accessible surface (*white surface*).

[Leu^5]enkephalin and the loss of the interaction between its free carboxyl group and Arg^{131} decrease its binding to wild-type NEP2, the affinity of naturally amidated substrates was not significantly affected by the loss of Arg^{131} (*i.e.* substance P and cholecystokinin-8). Taken together, these results suggest that, although C-terminal amidation of a peptide can hinder its binding to Arg^{131} of NEP2 S'_2 subsite, naturally amidated peptides can effectively bind this subsite through other interactions. Moreover, the endopeptidase activity of NEP2, similar to that of NEP (50), is unaffected by the loss of this active site arginine residue (*e.g.* angiotensin I), underlying the non-essential and very variable nature of this interaction. Variability again reflected by the binding of bradykinin that, although it possess a P'_2 arginine residue ($\downarrow$ Phe^8-Arg^9), which should be repelled by the positive charge of Arg^{131}, binds NEP2 and its R131M mutant with equally high affinity (Table II). The ensemble of these results not only validates the modeling process but confirms for the first time the implication of the Asn^{567} residue of NEP2 in its catalytic activity as well as that of Arg^{131} in the dipeptidyl carboxypeptidase activity of this metalloprotease.

The differences brought to light between the NEP and NEP2 S'_2 subsites could account for their related but distinct inhibitory profiles. Indeed, whereas NEP has a high affinity for compounds that possess a large hydrophobic moiety in either P'_1 and/or P'_2, NEP2 does not tolerate large side chains in P'_1. This is reflected by the affinities of compounds II and IV (biphenyl moiety in P'_1), which are 600 and 60 times more potent against NEP, respectively (Table III). Although these data suggest that differences between the two enzymes should lie within the P'_1 subsite, both the modeling and docking (Figs. 2 and 4) results provide another explanation to these data. Indeed, the docking of compound II in the active site of the NEP crystal (Fig. 4) reveals that the biphenyl moiety of this compound adopts a conformation where it partly fills the S'_2 subsite of the protease. This could provide an explanation for the loss of affinity, although still in the nanomolar range, of compound II *versus* compound IV toward NEP where the indole moiety in P'_2 of compound IV fills the S'_2 subsite of NEP and hinders binding of the P'_1 biphenyl moiety in the same subsite. Although NEP2 binds compounds with large indole moieties in P'_2 with high affinity (*e.g.* phosphoramidon and compound III), it does not bind compounds with biphenyl moieties in P'_1 whether they are with (compound IV) or without (compound II) large P'_2 moieties. These results suggest that, if the adopted conformation of the biphenyl moiety in the active site of NEP2 is the same as that of NEP, it does not fit as well in the NEP2 S'_2 subsite in which the presence of Ser^{133} and Leu^{739} could modify access or binding. This is further evidenced by the decrease in affinity between compounds III and IV (160-fold) in which the indole moiety in P'_2 is probably to fill the S'_2 subsite of NEP2.

Site-directed mutagenesis of the two differential amino acids in this subsite and transfection of these mutants yielded secreted active NEP2 mutants (Fig. 3 and Table I). Recently, we have compared the catalytic properties of NEP and NEP2 using a series of model and bioactive peptides (28) and have shown that, although they both bind the model fluorogenic substrate Suc-AAF-AMC with comparable affinities, for instance, the catalytic constant (k_{cat}) of NEP is approximately four times that of NEP2 (Table I). Although the kinetic values obtained with the S133G mutant of NEP2 were significantly different from those of wild-type NEP2, they were not any closer to those previously obtained for wild-type NEP, thus not allowing to infer a NEP/NEP2-differentiating function of this residue. Nevertheless, the significant decrease of affinity of the substrate toward this mutant does suggest that this residue may be involved in the binding of the substrate (or inhibitor). Whereas the specific activity of this latter mutant was significantly decreased, the ones of the L739G and S133G/L739G double mutant were both increased toward NEP values. Moreover, this effect was mainly the result of an increase in their catalytic activity, giving these mutants a NEP-like profile, *i.e.* both a high affinity and catalytic constant toward the model substrate. Furthermore, the pharmacological properties of these two mutants are shown to acquire NEP-like qualities toward discriminatory NEP/NEP2 compounds, the only exception being thiorphan. Indeed, the replacement of the large side chain of Leu^{739} by a glycine residue in S'_2 of NEP2 allows the binding of compounds I, II, and IV with affinities either closer to or identical to those of NEP. Values toward the double mutant (S133G/L739G) are either equal to or better, *i.e.* closer to those

of NEP, than the ones obtained with the L739G mutant, suggesting some kind of effect of the Ser^{133} residue on inhibitor binding, an effect that is particularly apparent with compounds that acquire better binding properties to the NEP2 double mutant than to NEP (*i.e. Compounds III* and *IV* in Table IV).

The ensemble of the results seem to point to the fact that specific interactions within a particular subsite depend on the nature of the residue as well as on the manner in which it is "presented," *i.e.* on the conformation of the substrate or inhibitor. For instance, the inhibitory potency of compound IV with an indole moiety in P'_2 position toward the S133G mutant is increased >10-fold toward a value closer to that of NEP, whereas the same P'_2 moiety in the context of the phosphoramidon molecule loses affinity toward this same mutant. Although the proposed model of the NEP2 active site may have some limits, as reflected by the results obtained with thiorphan on one hand and the ambiguous results of the S133G mutant on the other, it may be interesting to note that, in the cases of thiorphan and compound II, these ambiguous results can be explained by the unsuspected involvement of Arg^{131} in inhibitor binding, the removal of which (in the R131M mutant) abolishes their binding to NEP2. Furthermore, this observation seems to be specific to NEP2 as it was not previously observed with Arg^{102} mutants of NEP and as revealed by the recent co-crystallization of NEP with different inhibitory compounds, which show no charged residues of the NEP S'_2 subsite as being directly involved in inhibitor binding (51).

The template used here to model the NEP2 active site was that of NEP bound to phosphoramidon, an equipotent inhibitor of NEP and NEP2. Because enzymes, like receptors, adopt different conformational states when bound to different molecules (51), it is likely that this model, just as the crystal, may not allow the unraveling of all of the different residues involved in inhibitor (and substrate) binding. Nevertheless, the proposed three-dimensional structure of the NEP2 active site based on the x-ray structure of NEP together with site-directed mutagenesis results enabled us to put forward the first reasonably accurate active site model of NEP2, which provides important information for the synthesis of new specific inhibitory compounds of this protease. We have validated the function of Arg^{131} in the dipeptidyl carboxypeptidase activity of NEP2 as well as unraveled its function in the binding of some inhibitory compounds. The participation of Asn^{567} in both substrate binding (and to a lesser extent inhibitor) and hydrolysis is equally confirmed. Finally, Leu^{739} and Ser^{133} were identified and validated as unsuspected and important amino acids to the enzymatic specificity of NEP2.

Acknowledgments—We thank M. G. E. Dale and collaborators for providing the three-dimensional structure of hNEP.

REFERENCES

1. Ouimet, T., Facchinetti, P., Rose, C., Bonhomme, M. C., Gros, C., and Schwartz J. C. (2000) *Biochem. Biophys. Res. Commun.* **271,** 565–570
2. Ikeda, K., Emoto, N., Raharjo, S. B., Nurhantari, Y., Saiki, K., Yokoyama, M., and Matsuo, M. (1999) *J. Biol. Chem.* **274,** 32469–32477
3. Ghaddar, G., Ruchon, A. F., Carpentier, M., Marcinkiewicz, M., Seidah, N. G., Crine, P., Desgroseillers, L., and Boileau, G. (2000) *Biochem. J.* **347,** 419–429
4. Malfroy, B., Schofield, P. R., Kuang, W. J., Seeburg, P. H., Mason, A. J., and Henzel, W. J. (1987) *Biochem. Biophys. Res. Commun.* **144,** 59–66
5. Malfroy, B., Kuang, W. J., Seeburg, P. H., Mason, A. J., and Schofield, P. R. (1988) *FEBS Lett.* **229,** 206–210
6. Devault, A., Lazure, C., Nault, C., Le Moual, H., Seidah, N.G., Chretien, M., Kahn, P., Powell, J., Mallet, J., and Beaumont, A. (1987) *EMBO J.* **6,** 1317–1322
7. Xu, D., Emoto, N., Giaid, A., Slaughter, C., Kaw, S., DeWit, D., and Yanagisawa, M. (1994) *Cell* **78,** 473–485
8. Emoto, N., and Yanagisawa, M. (1995) *J. Biol. Chem.* **270,** 15262–15268
9. Lee, S., Zambas, E. D., Marsh, W. L., and Redman, C. M. (1991) *Proc. Natl. Acad. Sci. U. S. A.* **88,** 6353–6357
10. Du, L., Desbarats, M., Viel, J., Glorieux, F. H., Cawthorn, C., and Ecarot, B. (1996) *Genomics* **36,** 22–28
11. Valdenaire, O., Richards, J. G., Faull, R. L., and Schweizer, A. (1999) *Brain Res. Mol. Brain Res.* **64,** 211–221
12. Chothia, C., Gough, J., Vogel, C., and Teichmann, S. A. (2003) *Science* **300,** 1701–1703
13. Roques, B. P., Noble, F., Dauge, V., Fournie-Zaluski, M. C., and Beaumont, A. (1993) *Pharmacol. Rev.* **45,** 87–146
14. Turner, A. (1998) in *Handbook of Proteolytic Enzymes* (Barrett, A. J, Rawlings, N. D., and Woessner, J. F, eds) pp. 1080–1085, Academic Press, Orlando, FL
15. Kerr, M. A., and Kenny, A. J. (1974) *Biochem. J.* **137,** 477–488
16. Malfroy, B., Swerts, J. P., Guyon, A., Roques, B. P., and Schwartz, J. C. (1978) *Nature* **276,** 523–526
17. Matsas, R., Fulcher, I. S., Kenny, A. J., and Turner, A. J. (1983) *Proc. Natl. Acad. Sci. U. S. A.* **80,** 3111–3115
18. Gafford, J. T., Skidgel, R. A., Erdos, E. G., and Hersh, L. B. (1983) *Biochemistry* **22,** 3265–3271
19. Kenny, A. J., and Stephenson, S. L. (1988) *FEBS Lett.* **232,** 1–8
20. Schwartz, J. C., Gros, C., Lecomte, J. M., and Bralet, J. (1990) *Life Sci.* **47,** 1279–1297
21. Patey, G., De La Baume, S., Schwartz, J. C., Gros, C., Roques, B., Fournie-Zaluski, M. C., and Soroca-Lucas, E. (1981) *Science* **212,** 1153–1155
22. Mauborgne, A., Bourgoin, S., Benoliel, J. J., Hamon, M., and Cesselin, F. (1991) *Neurosci. Lett.* **123,** 221–225
23. Gros, C., Souque, A., Schwartz, J. C., Duchier, J., Cournot, A., Baumer, P., and Lecomte, J. M. (1989) *Proc. Natl. Acad. Sci. U. S. A.* **86,** 7580–7584
24. Roques, B. P., Fournie-Zaluski, M. C., Soroca, E., Lecomte, J. M., Malfroy, B., Llorens, C., and Schwartz, J. C. (1980) *Nature* **288,** 286–288
25. Baumer, P., Danquechin-Dorval, E., Bertrand, J., Vetel, J. M., Schwartz, J. C., and Lecomte, J. M. (1992) *Gut* **33,** 753–758
26. Bralet, J., and Schwartz, J. C. (2001) *Trends Pharmacol. Sci.* **22,** 106–109
27. Facchinetti, P., Rose, C., Schwartz, J. C., and Ouimet, T. (2003) *Neuroscience* **118,** 627–639
28. Rose, C., Voisin, S., Gros, C., Schwartz, J. C., and Ouimet, T. (2002) *Biochem. J.* **363,** 697–705
29. Deleted in proof
30. Pollard, H., Llorens-Cortes, C., Couraud, J. Y., Ronco, P., Verroust, P., and Schwartz, J. C. (1987) *Neurosci. Lett.* **77,** 267–271
31. Llorens, C., and Schwartz, J. C. (1981) *Eur. J. Pharmacol.* **69,** 113–116
32. Mauborgne, A., Bourgoin, S., Benoliel, J. J., Hirsch, M., Berthier, J. L., Hamon, M., and Cesselin, F. (1987) *J. Pharmacol. Exp. Ther.* **243,** 674–680
33. Oefner, C., D'Arcy, A., Hennig, M., Winkler, F. K., and Dale, G. E. (2000) *J. Mol. Biol.* **296,** 341–349
34. Hersh, L. B., and Morihara, K. (1986) *J. Biol. Chem.* **261,** 6433–6437
35. Pozgay, M., Michaud, C., Liebman, M., and Orlowski, M. (1986) *Biochemistry* **25,** 1292–1299
36. Benchetrit, T., Bissery, V., Mornon, J. P., Devault, A., Crine, P., and Roques, B. P. (1988) *Biochemistry* **27,** 592–596
37. Thompson, J. D., Higgins, D. G., and Gibson, T. J. (1994) *Nucleic Acids Res.* **22,** 4673–4680
38. Henikoff, S., and Henikoff, J. G. (1992) *Proc. Natl. Acad. Sci. U. S. A.* **89,** 10915–10919
39. Case, D. A., Pearlman, D. A, Caldwell, J. W., Cheatham, D. E., III, Ross, W. S., Simmerling, C. L., Darden, T. A., Merz, K. M., Stanton, R. V., Cheng, A. L., Vincent, J. J., Crowley, M., Tsui, V., Radmer, R. J., Duan, Y., Pitera, J., Massova, I., Seibel, G. L., Singh, U. C., Weiner, P. K., and Kollman, P. A. (1999) *AMBER 6.0*, University of California, San Francisco, CA
40. Cornel, W. D., Cieplak, P., Bayly, C. I., Gould, I. R., Merz, J. K. M., Ferguson, D. M., Spellmeyer, D. M., Fox, T., Caldwell, J. W., and Kollman, P. A. (1995) *J. Am. Chem. Soc.* **117,** 5179–5197
41. Rognan, D., Mukhija, S., Folkers, G., and Zerbe, O. (2001) *J. Comput. Aided Mol. Des.* **15,** 103–115
42. Bissantz, C., Folkers, G., and Rognan, D. (2000) *J. Med. Chem.* **43,** 4759–4767
43. Jones, G., Wilett, P., Glen, R. C., Leach, A. R., and Taylor, R. (1997) *J. Mol. Biol.* **267,** 727–748
44. Lemay, G., Waksman, G., Roques, B. P., Crine, P., and Boileau, G. (1989) *J. Biol. Chem.* **264,** 15620–15623
45. Dion, N., Le Moual, H., Fournie-Zaluski, M. C., Roques, B. P., Crine, P., and Boileau, G. (1995) *Biochem. J.* **311,** 623–627
46. Dion, N., Cohen, P., Crine, P., and Boileau, G. (1997) *FEBS Lett.* **411,** 140–144
47. Malfroy, B., and Schwartz, J. C. (1984) *J. Biol. Chem.* **259,** 14365–14370
48. Bateman, R.C., Jr., Jackson, D., Slaughter, C. A., Unnithan, S., Chai, Y. G., Moomaw, C., and Hersh, L. B. (1989) *J. Biol. Chem.* **264,** 6151–6157
49. Beaumont, A., Le Moual, H., Boileau, G., Crine, P., and Roques, B. P. (1891) *J. Biol. Chem.* **266,** 214–220
50. Kim, Y. A., Shriver, B., Quay, T., and Hersh, L. B. (1992) *J. Biol. Chem.* **267,** 12330–12335
51. Oefner, C., Roques, B. P., Fournie-Zaluski, M.-C., and Dale, G. E. (2004) *Acta Crystallogr. Sect. D Biol. Crystallogr.* **60,** 392–396